Using Emulated Bistatic Radar in Highly Coherent Applications: Overview of Results

James Palmer[1,2], Marco Martorella[3], Brad Littleton[4], and John Homer[1]
1 – The School of ITEE, The University of Queensland, AUSTRALIA
2 – The Defence Science and Technology Organisation (DSTO), AUSTRALIA
3 – Dept. of Information Engineering, The University of Pisa, ITALY
4 – The School of Physics, The University of Queensland, AUSTRALIA
Email: james.palmer@dsto.defence.gov.au

In this paper, the application of an Emulated Bistatic Radar's geometry to highly coherent signal processing techniques is discussed. This paper presents a brief overview of the theoretical, simulated and experimental results processed to date for synthetic aperture radar imaging, inverse synthetic aperture radar imaging and interferometric signal processing using the three paths inherent in an Emulated Bistatic Radar. A brief discussion about the signal models employed for these processing techniques is also given, and considerations about future simulated, experimental and theoretical research are provided.

1. INTRODUCTION

In this paper, the use of an Emulated Bistatic Radar (EBR) system with highly coherent radar imaging techniques, such as synthetic aperture radar (SAR), inverse SAR (ISAR), and interferometry (for target height estimation) is discussed. The paper shall be structured as follows: in Section 2, we briefly discuss the theory behind the original application of the EBR; in Section 3, the EBR configuration is discussed with respect to an interferometric target height estimation scenario; Section 4 sees the application of Synthetic Aperture Radar (SAR) processing to each of the EBR signal propagation paths; Section 5, similarly, applies Inverse Synthetic Aperture Radar (ISAR) image processing; and finally Section 6 concludes this report.

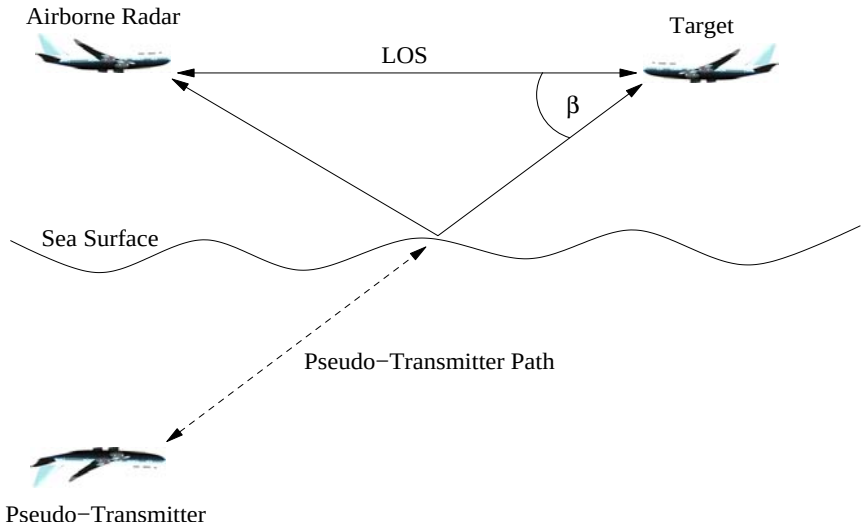

Figure 1: A monostatic radar emulating a bistatic radar via a sea surface reflected path

Palmer, J.; Martorella, M.; Littleton, B.; Homer, J. (2006) Using Emulated Bistatic Radar in Highly Coherent Applications: Overview of Results. In *Bistatic-Multistatic Radar and Sonar Systems* (pp. 18-1 – 18-10). Meeting Proceedings RTO-MP-SET-095, Paper 18. Neuilly-sur-Seine, France: RTO. Available from: http://www.rto.nato.int/abstracts.asp.

An EBR system (shown in Figure 1) is an airborne or ground-based monostatic radar that is configured to emulate a bistatic/multistatic radar; and has been discussed previously by the authors in [1-4]. Bistatic radar emulation is achieved by employing the reflective nature of the sea's surface to create a 'pseudo-transmitter'. This creates three signal paths: the double direct (real Monostatic Radar (MR) path); the direct-indirect (Emulated Bistatic Radar (EBR) path); and the double indirect (Emulated Monostatic Radar (EMR) path).

2. EBR THEORY

The Emulated Bistatic Radar was originally developed as an alternative detection approach to standard monostatic radar. Part of the motivating force behind this theoretical development was that the bistatic RCS of aircraft-type targets, and stealthily aircraft in particular, are generally much higher than their monostatic RCS. However, standard bistatic radars suffer some limitations that are much less significant in a monostatic platform. For example, synchronisation between the transmitter and receiver can be a significant problem due to the spatial separation of these elements; however, in monostatic radar these elements are typically collocated and generally share a common stable local oscillator, and therefore suffer no such concerns. Also, the costs associated with operating a dedicated bistatic airborne-based detection platform are much greater than an equivalent monostatic platform, as only one aircraft is required. An EBR, on the other hand, combines these advantages provided by both the standard monostatic radar and bistatic radar, without significantly increasing the computational cost or complexity.

For an airborne platform, with an EBR configured radar, to be competitive against a standard monostatic configured radar, the improvement that results from the change in RCS of the target must account for the loss that occurs due to the increase in radar path length, and the losses that result from the inclusion of the sea's surface in the signal propagation path. This requirement is stated, mathematically, as follows:

$$\frac{\sigma_B}{\sigma_M} > \frac{R_B^2 L_B F_M^2}{R_M^2 L_M F_B^2} \quad \textbf{1}$$

where σ_B is the bistatic RCS, σ_M is the monostatic RCS, R_B is the indirect path propagation distance, R_M is the direct path propagation distance, L_B are the EBR losses, L_M are the monostatic losses and F_M and F_B are the monostatic and bistatic path propagation factors.

In order for the EBR to function as a viable detection approach, the sea surface reflected signal must also maintain some level of coherence and must not reflect radiation in an entirely diffuse manner. Extensive research in the remote sensing field, for e.g. [5, 6], has repeatedly demonstrated the detectability of sea surface reflected GNSS, in particular GPS, signals. This research indicates that sea surface forward scattered signals do maintain a level of coherence and do have preferential scatter in the forward scatter, or specular, direction. Simulation based analysis has been conducted in order to further understand the impact of sea surface on the reflected path signal, but this work is still ongoing and fully conclusive results have yet to be reached.

3. EBR INTERFEROMETRY

The realisation that sea surface forward scattered signals maintain at least partial coherence led to the consideration of other signal processing techniques that could take advantage of this. As a result, target height estimation using interferometry was considered.

Interferometry in airborne radar is a well understood phenomenon that allows the estimation of target's cross range dimension (typically height). Interferometric processing requires the use of either two antennas, a large antenna (with a displaced phase centre beam forming capability) or the use of repeat pass

signal reception with a slight change in the subsequent antenna location. All of these techniques, however, require either more complicated hardware or an antenna location change. The use of the EBR geometry for interferometric applications, on the other hand, will allow phase interferometry to occur without requiring a significant increase in hardware complexity or a physical change of antenna location.

The combination of an EBR's geometry with interferometry allows several interferograms to be processed. The work of Griffiths et al [7], in particular, provides a good platform from which we can consider the application of interferometric processing techniques to an airborne or shipborne EBR. Using their work as a basis, we extend the interferometric signal model to an EBR's geometry as follows:

$$\phi_D = \frac{2\pi}{\lambda}\left(R_{MR} - R_{EMR}\right) = \frac{2\pi}{\lambda}\left[R_{MR} - \sqrt{B^2_{L_{MR-EMR}} + R^2_{MR} - 2R_{MR}B_{L_{MR-EMR}}\cos(\frac{\pi}{2} + \theta_{MR})}\right] \quad (2)$$

where ϕ_D represents the phase difference between the paths of the interferogram being considered, and all other parameters are defined in Figure 2. By rearranging Eqn 2, we can then determine the angle of the target's scatterers position, via:

$$\theta_{MR} = \arccos\left(\frac{B_{L_{MR-EMR}}}{2R_{MR}} - \frac{\phi_D^2\lambda^2}{8\pi^2 R_{MR}B_{L_{MR-EMR}}} + \frac{\phi_D\lambda}{2\pi B_{L_{MR-EMR}}}\right) - \frac{\pi}{2} \quad (3)$$

and their corresponding Cartesian coordinates via:

$$y = y_{MR} + R_{MR}\sin\left(\theta_{MR} + \theta_{B_L}\right) \quad (4)$$

$$z = z_{MR} - R_{MR}\cos\left(\theta_{MR} + \theta_{B_L}\right) \quad (5)$$

In Eqns 2-5, it has been assumed that the interferogram being considered is using the MR and EMR signal paths; the MR to EBR and EBR to EMR interferograms' equations can also be determined from Eqns 2-5 through the appropriate substitutions. For example, to change to a MR to EBR interferogram, the EMR subscripts need to be changed to EBR in Eqn 3.

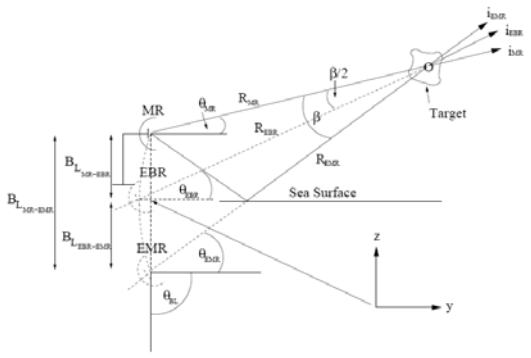

Figure 2: An Interferometric EBR System's Geometry

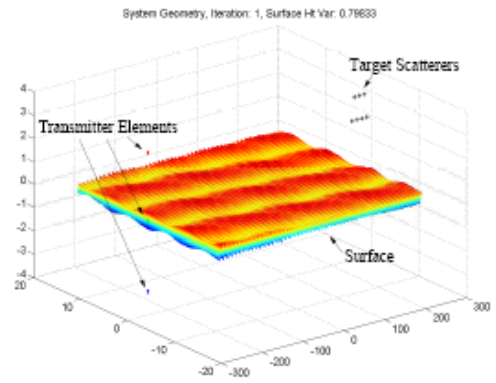

Figure 3: The EBR Interferometric simulation geometry

Some example simulated results, taken from the simulation setup depicted in Figure 3, are given in Figure 4 and Figure 5. In these figures, a 2.5a and 5a Pierson Moskowitz [8] sea state was used and the simulation generated three interferograms corresponding to the three available path pairs. In Figure 4 and Figure Figure 5, two sets of results have been included; those that indicate reasonable agreement, and those that demonstrate poor agreement between the interferometric estimates and the actual positions. It

should be noted that even in the reasonable agreement case, there still remains a bias that results in a tilt in the image estimates. The cause of this bias has yet to be fully determined.

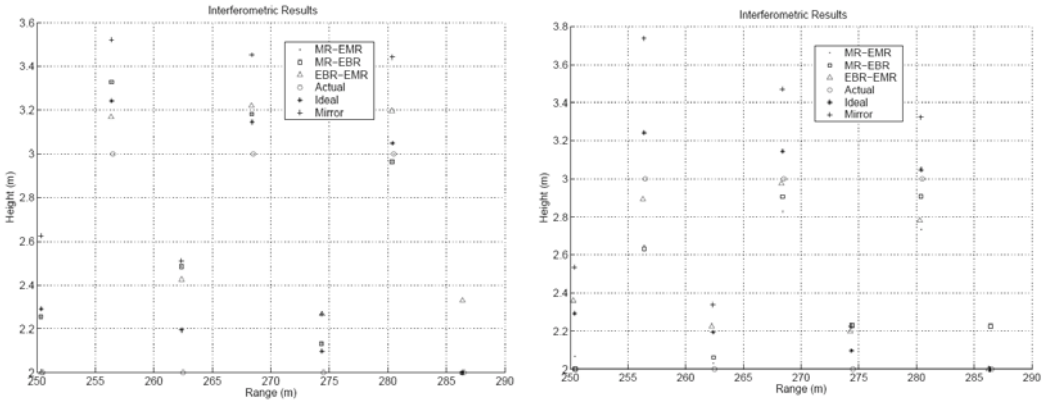

Figure 4: Examples of reasonable target height estimation at Sea State 2.5a and 5a

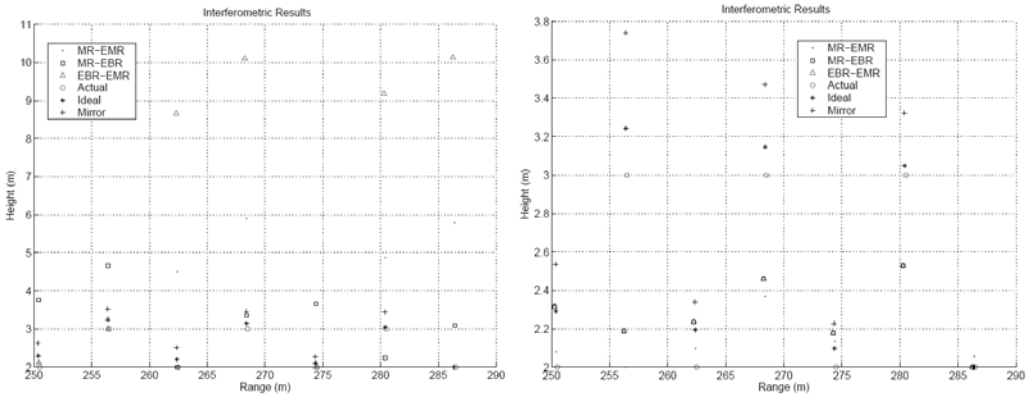

Figure 5: Examples of poor target height estimation at Sea State 2.5a and 5a

4. EBR SYNTHETIC APERTURE RADAR

Synthetic Aperture Radar (SAR) is another signal processing technique that was considered in conjunction with an EBR's geometry. Once more, we shall initially consider an Emulated Bistatic SAR signal model, and then look at some experimental results. The complex basebanded received signal from a point scatterer illuminated with a linear FM radar can be written as:

$$r\left(t_{fast},x\right)=\rho\left(\tilde{r_s}\right)e^{-j\frac{2\omega_0 R(x)}{c}}\overbrace{a\left(t_{fast}-\frac{2R\left(x\right)}{c}\right)\cdot e^{j\frac{1}{2}\mu\left[t_{fast}-\frac{2R(x)}{c}\right]^2}}^{SlantRange}\cdot\underbrace{rect\left(\frac{x-x_s}{L/2}\right)\cdot e^{-j\left[\frac{2\omega_0\dot{R}(x)}{cv}(x-x_s)+\frac{2\omega_0\ddot{R}(x)}{cv}(x-x_s)^2\right]}}_{Azimuth} \quad (6)$$

A full description of the parameters given in Equation 6 are not provided here due to space constraints and may instead be found in [9]. Suffice it to say, it is the range components in Eqn 6 that are affected by the EBR geometry, and the received signal for each signal propagation path can be found by substituting the following equations, and their subsequent derivations, into Eqn 6 as appropriate:

$$R_{MR}\left(x\right)=R_{Direct}+R_{Direct} \quad (7)$$

$$R_{EBR}(x) = R_{Direct} + R_{Indirect} \quad (8)$$

$$R_{EMR}(x) = R_{Indirect} + R_{Indirect} \quad (9)$$

where R_{Direct} represents the one way monostatic radar path, and $R_{Indirect}$ represents the one way EMR path, as shown in Figure 6.

Real world SAR campaign data, provided by NASA's JPL, of the San Francisco bay region, and in particular of the Golden Gate Bridge, demonstrates the reception of the three radar signal paths. Figure 6 shows the experimental configuration employed for this experiment, whilst Figure 7 shows the equivalent signal propagation and imaging paths. This data was collected as part of JPL's AIRSAR campaign in May 1999, and the ENVI processed results are shown in Figure Figure 8 – Figure Figure 13.

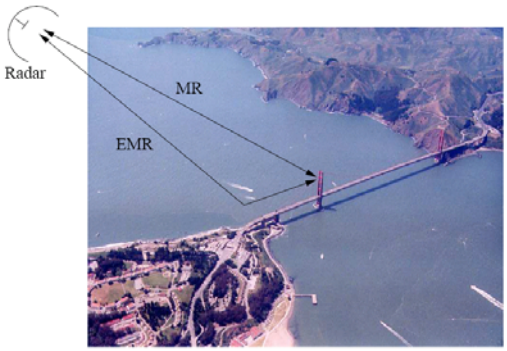

Figure 6: Experimental Geometry

Figure 7: Equivalent Imaging Radar configurations

Figure 8: C-Band HH Polarised

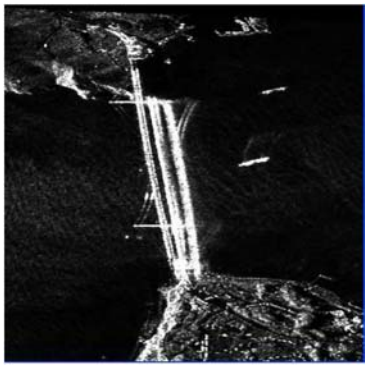

Figure 9: C-Band VV Polarised

Figure 10: C-Band HV Polarised

Figure 11: L-Band HH Polarised

Figure 12: L-Band VV Polarised

Figure 13: L-Band HV Polarised

Visual analysis comprising the polarisations and frequency bands of the processed data displayed inFigure 8 - Figure 13 demonstrate that a greater signal to sea clutter ratio exists for the HH polarisation than the VV and that L Band may be slightly less susceptible to indirect path blurring than C Band, although this is only a marginal improvement. Further experimental studies are required before fully conclusive results may be determined.

EBR INVERSE SYNTHETIC APERTURE RADAR

In this section, the geometric considerations required to generate ISAR images using the experimental campaign data obtained from the Australian Defence Science and Technology Organisation (DSTO) will be briefly considered. The signal model employed in the formation of ISAR images is fully described in [4] and briefly described below:

$$S_R(f,t) = rect\left(\frac{t}{T_{obs}}\right) rect\left(\frac{f-f_c}{B}\right) \int_V \zeta(\underline{x}) e^{j\varphi(\underline{x},f,t)} d\underline{x} \qquad \textbf{10}$$

where S_R is the post-processed signal, $\varphi_{MR}(x,f,t) = \frac{4\pi f}{c}\left[R_{MR}(t) + x \cdot i_{MR}(t)\right]$ is the monostatic radar phase component, $\varphi_{EMR}(x,f,t) = \frac{4\pi f}{c}\left[R_{EMR}(t) + x \cdot i_{EMR}(t)\right]$ is the emulated monostatic radar phase and $\varphi_{EBR}(x,f,t) = \frac{(\varphi_{MR}(x,f,t) + \varphi_{EMR}(x,f,t))}{2} = \frac{2\pi f}{c}\left[2R_{MR}(t) + \Delta R_{MR}(t) + K(t)x \cdot i_{EBR}(t)\right]$ is the emulated bistatic radar phase component.

The data discussed here was collected during an airborne ISAR imaging campaign conducted in the early 1990s by DSTO and was processed using an autofocusing algorithm developed by the University of Pisa [10]. A photo of the cargo ship that was imaged in this trial is given in Figure 14. Figure 15 – Figure Figure 19 display the results from one portion of this trial. In Figure 15, the autofocussing algorithm was set to cease processing at a predefined iteration limit, resulting in all three images being simultaneously visible. Figure 16 and Figure Figure 17 show the truncated EBR path image taken from the initial partially focussed and the corresponding isolated refocussed image. Similarly, Figure 18 and Figure Figure 19 do likewise for the EMR image path.

Figure 14: A photo of the ship imaged in this trial

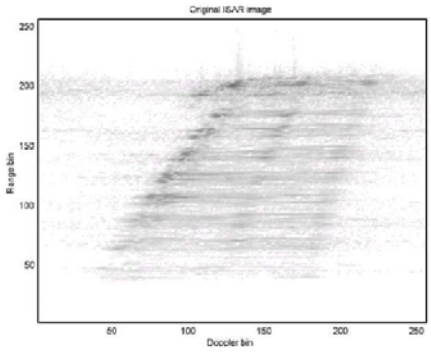

Figure 15: Initial partially focussed image

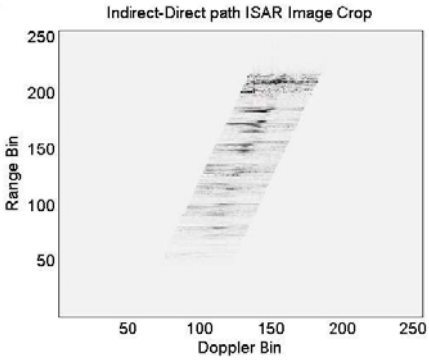

Figure 16: Truncated EBR Path Image

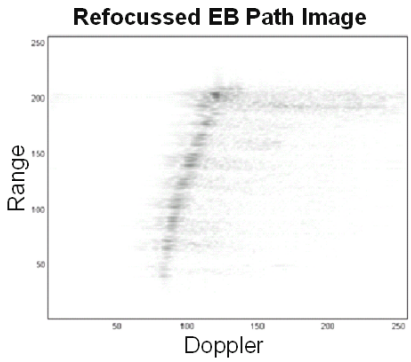

Figure 17: Refocussed EBR Path Image

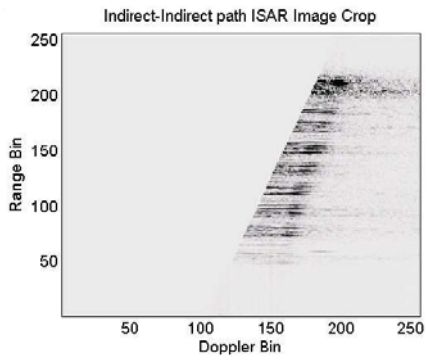

Figure 18: Truncated EMR Image

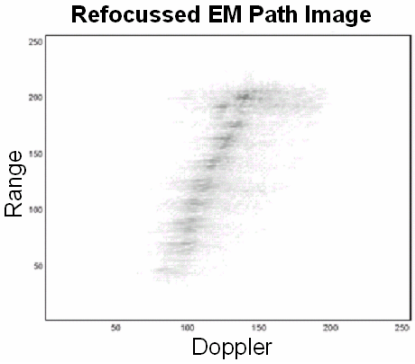

Figure 19: Refocussed EMR Path Image

In Figure 20 and Figure Figure 21, partially focussed images taken from different segments of the trial are displayed. These figures further demonstrate the variation in range and Doppler characteristics that may be seen in EBR images.

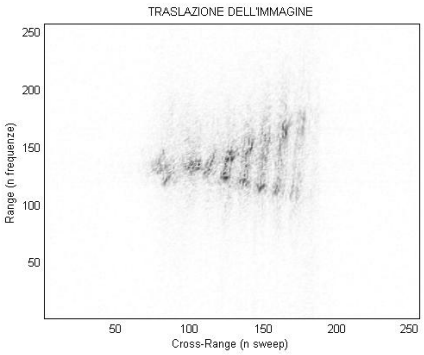

Figure 20: Alternate ISAR Image Plane Projections

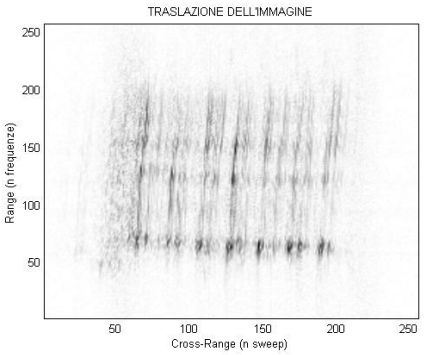

Figure 21: Range Separated Image Planes

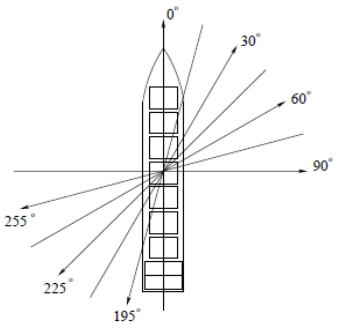

Figure 22: Collection run directions with respect to ship

Visual analysis of the results taken from the 7 data sets collected for this trial reveals that EBR images are more likely at certain imaging geometries. Each data set corresponds to a specific flight angle, with respect to the ship's heading, as shown in Table 1 and displayed in Figure 22. In Table 1 the "Multi-Image frame sets" column refers to the number of frame sets in the partially processed image data that produced three observable (MR, EBR, EMR) images. As can be seen in Table 1, the optimum flight direction with respect to the imaged ship's heading is clearly centred on the 45^{O} angle, and decreases as the flight direction tends toward either a broadside view or an end on angle with respect to the ship. These preliminary results indicate that the probability of recording images for each of the three EBR paths appears to improve when the target is imaged from a 45^{O} direction to its heading. However, as this analysis only considers one target with a relatively constant heading with respect to wave propagation direction and on a constant sea state, more analysis is required with a variety of targets, sea states, and imaging angles before this preliminary conclusion can be confirmed.

Table 1: Aspect Angle and Range

Data Set No.	Aspect Angle	Multi-Image frame sets
1	0°	9
2	15°(195°)	12
3	30°	15
4	45°(225°)	15
5	60°	17
6	75°(255°)	11
7	90°	0

5. CONCLUSIONS

In this paper, we have presented a brief overview of the application of an Emulated Bistatic Radar to several highly coherent imaging techniques; namely, interferometric signal processing, Synthetic Aperture Radar imaging, and Inverse Synthetic Aperture Radar imaging. A brief background to the EBR was initially provided, which looked at the original design purpose of the EBR and discussed some of its

advantages over standard monostatic and bistatic detection approaches. Following this, each processing technique was considered, with a brief overview of the signal models employed for each approach and either simulated or real world results presented. From these results, some conclusions were made about maximising the occurrence or clarity of achieving EBR images, and required future work was discussed.

6. REFERENCES:

1. Palmer, J., J. Homer, and B. Mojarrabi. *Improving on the monostatic radar cross section of targets by employing sea clutter to emulate a bistatic radar*. in *IGARSS 2003. 2003 IEEE International Geoscience and Remote Sensing Symposium. Proceedings, 21-25 July 2003*. 2003. Toulouse, France: IEEE.
2. Palmer, J., M. Martorella, and I.D. Longstaff. *Airborne ISAR Imaging using the Emulated Bistatic Radar System*. in *EUSAR 2004 Conference*. 2004. Ulm, Germany.
3. Palmer, J. and J. Homer. *SAR Generation through Bistatic Radar Emulation*. in *EUSAR 2004 Conference*. 2004. Ulm, Germany.
4. Palmer, J., et al., *ISAR imaging using an emulated multistatic radar system.* Aerospace and Electronic Systems, IEEE Transactions on, 2005. **41**(4): p. 1464-1472.
5. Zavorotny, V.U. and A.G. Voronovich, *Scattering of GPS signals from the ocean with wind remote sensing application.* IEEE Transactions on Geoscience and Remote Sensing, 2000. **38**(2, pt.2): p. 951-64.
6. Ruffini, G., et al., *GNSS-OPPSCAT WP1000 ESA Report : Remote Sensing of the Ocean by Bistatic Radar Observations: a Review*. 1999, IEEC: Barcelona.
7. Griffiths, H.D., et al. *Aircraft-borne interferometric SAR for 3-D high-resolution radar imaging*. in *IEE Electronics Division Colloquium on Radar and Microwave Imaging Techniques, Nov 16 1994*. 1994. London, UK: IEE, Stevenage, Engl.
8. Moskowitz, P.-. *Sea State Definition Table*. 2005, Resolute Weather.
9. Gunawardena, A.U.A.W., *Wave equation based synthetic aperture radar processing with applications to ground penetrating radar*. 1997: [St. Lucia],. p. 146 l :.
10. Martorella, M., F. Berizzi, and B. Haywood, *Contrast maximisation based technique for 2-D ISAR autofocusing.* IEE Proceedings: Radar, Sonar and Navigation, 2005. **152**(4): p. 253-262.